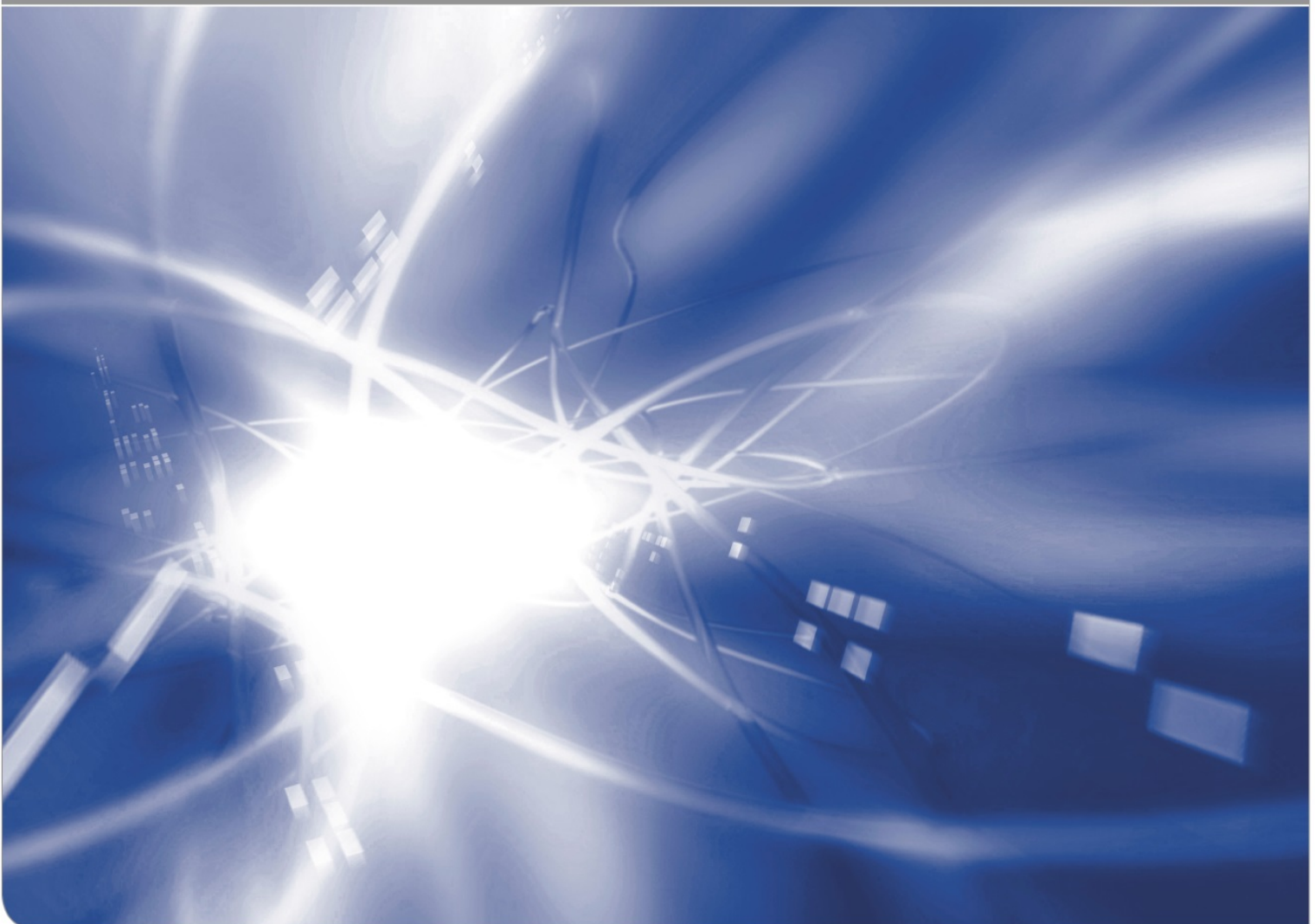# Error sources and geometry effects in DCDC-tests

G. Schell, G. Rizzi, P. Hettich, P. Zielonka, S. Wagner, T. Fett

Institut für Angewandte Materialien, Karlsruher Institut für Technologie (KIT)

Abstract

The main advantages of DCDC-specimens are the completely stable crack extension after spontaneous crack initiation due to the decreasing stress intensity factor with increasing crack length and a very high path stability due to the strongly negative T-stress term.

In this report, several possible error sources occurring in DCDC-tests are addressed:

- End effects in short specimens.
- Differently long cracks at both sides of the drill hole.
- Slight offset of the hole and the crack.
- Non-symmetrical loading,

Contents

1. Introduction

The main advantages of DCDC-specimens are the completely stable crack extension after spontaneous crack initiation due to the decreasing stress intensity factor with increasing crack length and a very high path stability due to the strongly negative T-stress term. This specimen, so far predominantly applied to glass, can be used also for high-strength materials as silicon nitrides and should allow R-curve measurements $K_R(\Delta a)$ over large crack extensions Δa. In this report possible error sources are addressed:

- End effects in short specimens,
- differently long cracks at both sides of the drill hole,
- slight offset of the hole and the crack,
- non-symmetrical loading,

2. Stress intensity factor solutions from literature

The "double cleavage drilled compression" (DCDC) specimen is a rectangular bar with a circular hole in its centre that is loaded by compressive stresses (Fig. 1a). Stress intensity factor solutions for the DCDC specimen are available in literature. The stress intensity factor of the symmetric test specimen, $b/R=0$ in Fig. 6, was determined for $H/R=4$ by many investigators, e.g. by Janssen [1], He et al. [2], Lardner et al. [3], Fett et al. [4,5], and for $H/R=3.75$ by Cai et al. [6], Michalske and Fuller [7], Michalske et al. [8].

Stress intensity factor results by Janssen [1] are given as

$$K_I = \frac{p\sqrt{R}}{0.375\dfrac{a}{R}+2} \tag{2.1}$$

The solution by He et al. [2] is

$$\frac{|p|\sqrt{\pi R}}{K_I} = \frac{1}{F} = \frac{H}{R} + \left[0.235\frac{H}{R} - 0.259\right]\frac{a}{R} \tag{2.2}$$

The same geometric function was confirmed by Lardner et al. [3].
The solution by Fett et al. [4,5]

$$\frac{1}{F} = -0.37 + 1.116\frac{H}{R} + \left[0.216\frac{H}{R} - 0.1575\right]\frac{a}{R} \tag{2.3}$$

Figure 2a shows these solutions. A description including term proportional $(a/R)^2$ was proposed by Pallares et al. [9]. An evaluation suggested by Sammis and Ashby [10] is obviously wrong as had been stated early by Michalske et al. [8]. Michalske et al. compared their results from FE-computations on a specimen with $H/R=3.75$ with

results from [10]. Very large deviations up to a factor of 6 were found as can be seen from Fig. 2b.
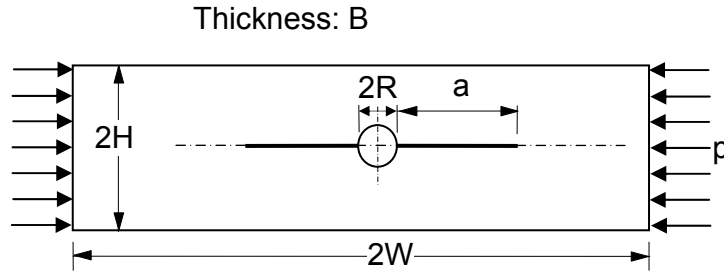
Thickness: B

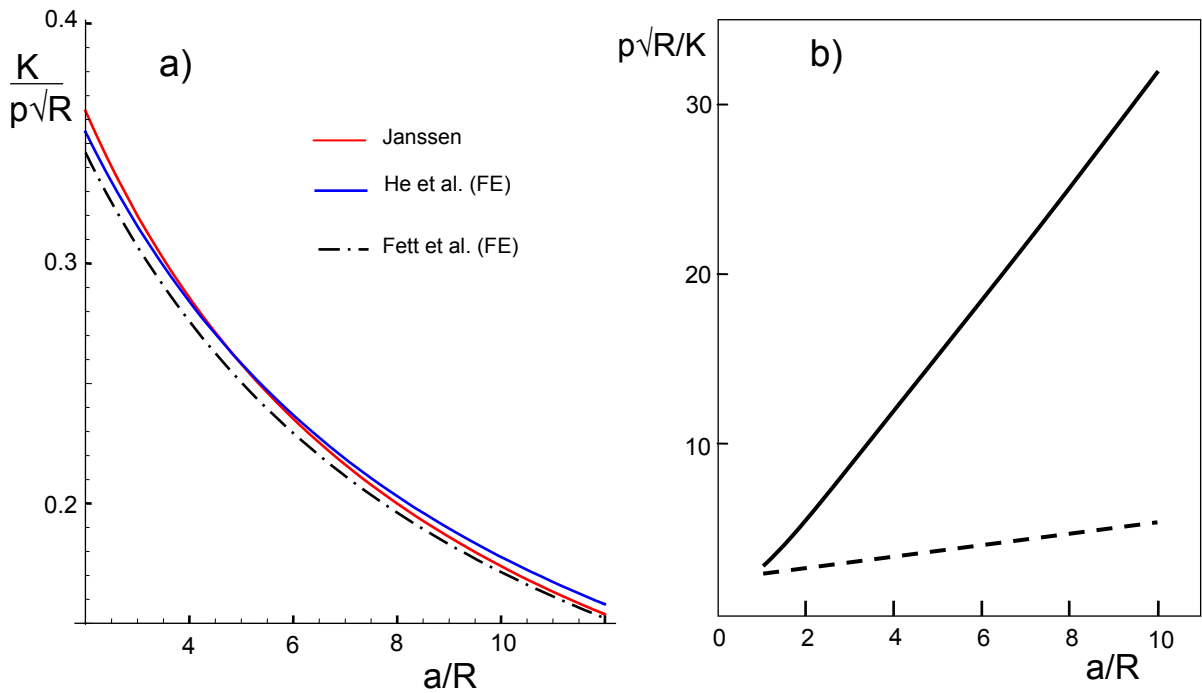**Fig. 1** a) The DCDC specimen (geometric data),

Fig. 2 a) Influence of crack length on stress intensity factors, b) Comparison of the solution by Sammis and Ashby [10] (dashed line) with a FE-solution for H/R=3.75 by Michalske et al. [8] (solid curve).

3. Limit-case behaviour

3.1 Short-crack behaviour

The stress intensity factors for short cracks with $a/R<2$ were computed in [11]. Figure 3a shows the FE-results, F_{FE} as the circles together with eq.(2.3) extended to $a/R\rightarrow0$ indicated by the dashed line. The squares represent results obtained via the weight function method. The red curve part can be expressed for the region $a/R\geq0.5$ by the simple correction term ΔF

$$F = F_{FE} + \Delta F , \quad \Delta F = 0.091\exp\left[-2.22\frac{a}{R}\right] \tag{3.1}$$

From Fig. 3b it becomes evident that an initially spontaneous crack extension must take place, starting from cracks on the hole. Let us assume a crack of size a_0 intro-

2

duced during the drilling procedure. With increasing load, the stress intensity factor of this crack increases monotonously. In the same way the energy release rate G increases due to $G \propto K^2$. The extension of the initial crack can be described in the same way as crack extension under thermal shock conditions. When the critical stress intensity factor $K=K_{Ic}$ or the critical energy release rate $G=G_c$ are reached, the crack propagates spontaneously. It would normally stop, when K again falls below K_{Ic}, or G below G_c. Then the crack depth a_1 is reached. Since the excess energy represented by the area ΔG becomes free in the crack propagation process, the crack will not necessarily stop at a_1 but will exceed this value. From this point of view, a_1 is a lower limit size for the crack arrest situation. This limit value is exceeded in most cases. A maximum crack a_2 will be reached, when all excess energy ΔG has been transformed into new crack surfaces. The condition for this is that the blue hatched area equals the red one. The crack a_2 is an upper limit, because not all excess energy can be converted in crack surface energy. Parts of the energy are converted into heat and acoustic energy (accompanied by an audible cracking noise). Consequently, the crack size must be in the interval $a_1 \leq a \leq a_2$. Completely stable crack propagation must occur if the initial crack is larger or equal to the distance of the maximum in the G-a curve. In this case no excess energy is available for spontaneous crack propagation.
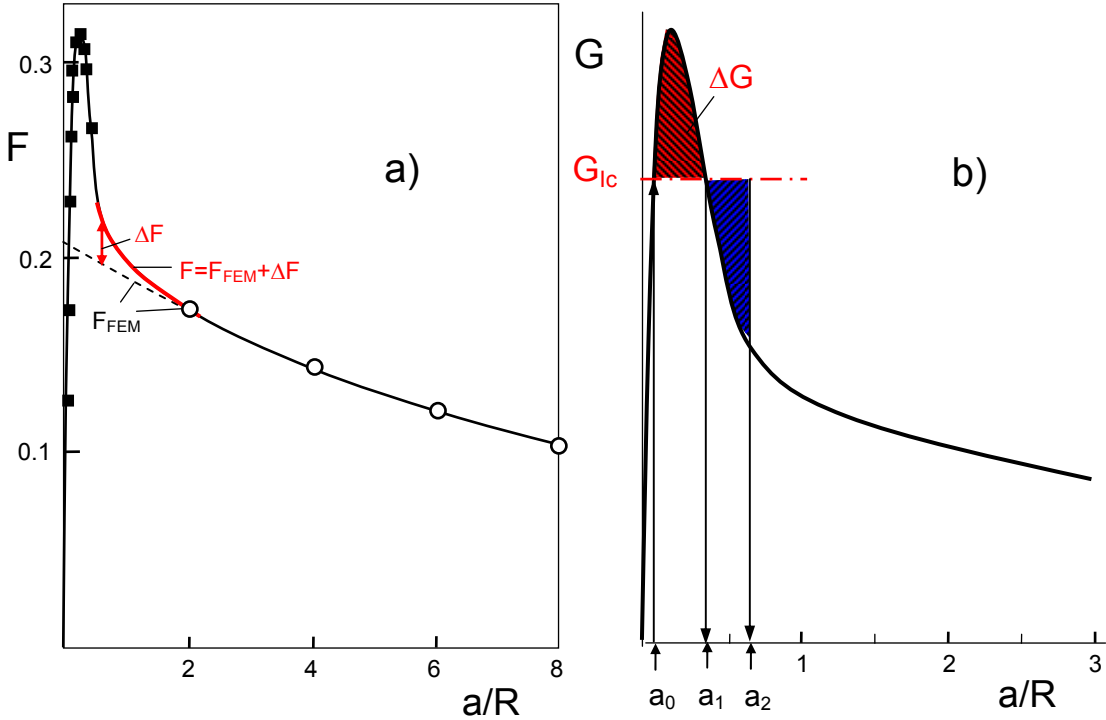
Fig. 3 a) Geometric function for the stress intensity factor for short cracks, circles: FE-results, squares: results obtained with the weight function method in [11], red curve part represents the correction by eq.(3.1), b) energy release rate representation used for explanation of the initial spontaneous crack formation: a_0 initial crack due to drilling, a_1 lower limit size of a crack after reaching the critical load, a_2 upper limit size when all excess energy (red hatched area) has been used for creation of new crack surfaces.

3

3.2 Long-crack behaviour

The relations mentioned in Section 3.1 are valid for the standard geometry with $W/H=10$. For specimens with reduced lengths, additional FE-computations were performed. The deviations from the standard solution K_0 obtained for the large "standard length" of $W_0=10H$ and $R=H/4$ are shown in Fig. 4a. Figure 4b represents the same results in dependence of the crack-tip distance from the end surface d. For decreasing distance from the end the stress intensity factor increases strongly. For a tolerated deviation of 1%, the distance from the end surfaces should be $d>1.75\,H$.

The curve through the data points can roughly be expressed by

$$K \approx K_0\left(1+14.45\exp\left[-4.23\frac{d}{H}\right]\right) \tag{3.2}$$

Results for a wide variation of geometries included end effects are given by Pallares et al. [9].
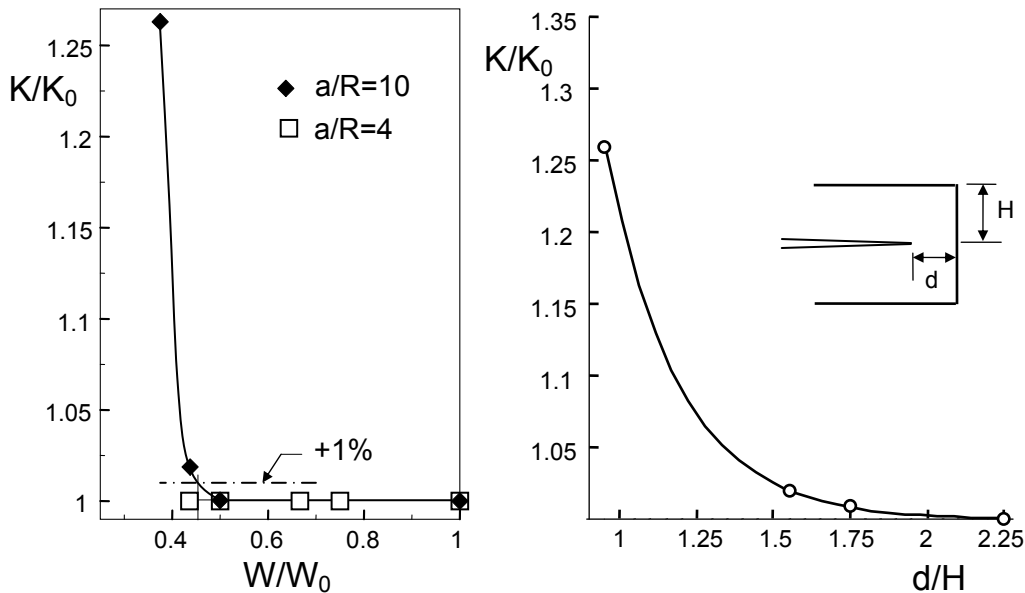
Fig. 4 a) Influence of the specimen length on the stress intensity factor (K_0=stress intensity factor for "standard geometry" $W_0=10\,H$, $H=4\,R$), b) results of Fig. 4a plotted vs. the crack-tip distance from the end faces.

4 Non-symmetrically grown cracks

Cracks may be generated during loading, which are not exactly symmetric exhibiting different lengths a_0 and a_1 (Fig. 5a). At the longer crack, the stress intensity factor is reduced. Finite element results for such different cracks are shown in Fig. 5b as the squares [5]. A straight-line fit of these data yields

$$F(a_1) \cong F(a_0)-0.13(\tfrac{a_1}{a_0}-1) \tag{4.1}$$

where $F(a_0)$ is the geometric function for two cracks with identical length of a_0, given by eqs.(2.1-2.1).
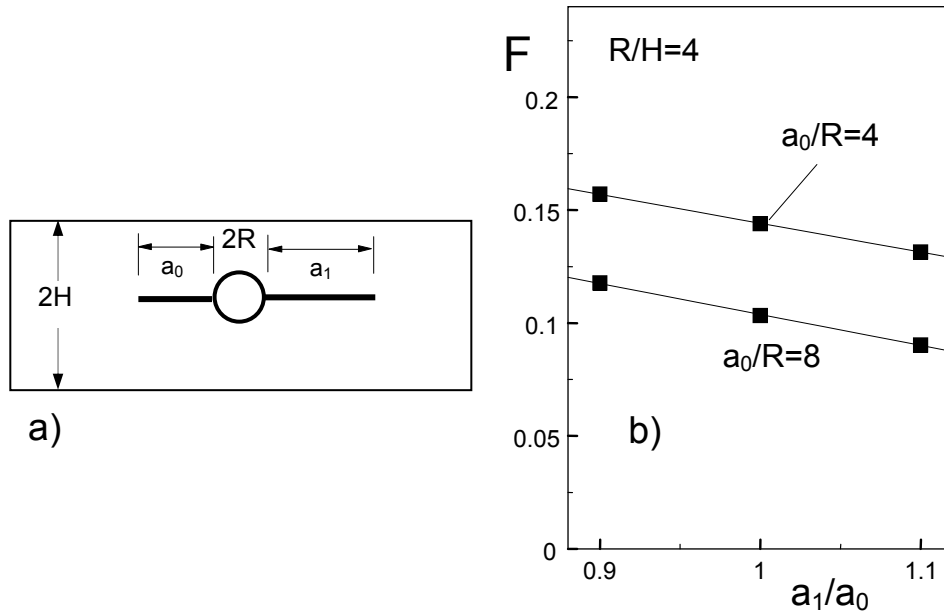
Fig. 5 a) Non-symmetric cracks, b) influence on the stress intensity factor.

5 Eccentricity

5.1 Offset of hole <u>and</u> crack

Due to unavoidable manufacturing tolerances small eccentricities of the hole location are possible. On the other hand it can be of interest to generate mixed-mode stress intensity factor loading. In this case, the eccentricity, b, in Fig. 6 is large. Mixed-mode stress intensity factors are given in [5]. In this report only small eccenticities are considered.
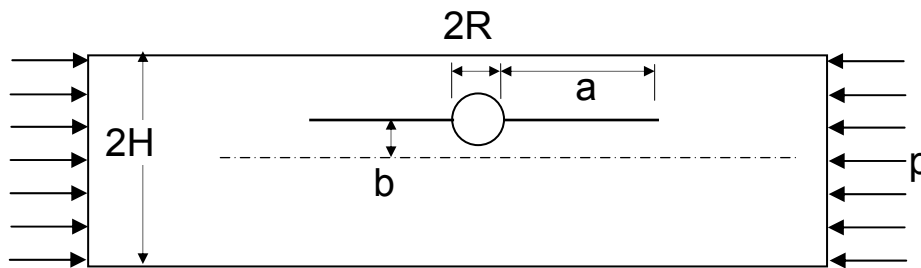

Fig. 6 DCDC specimen with an offset of the hole <u>and</u> the crack.

The numerical results of mode-I stress intensity factors from [5] for small offsets of $|b/R| \leq 0.2$ and the commonly used geometry of $H/R = 4$ can be expressed by the relation

$$F_{\mathrm{I}} \cong F_{\mathrm{I},0}\left[1+\left(0.122-0.003\frac{a}{R}\right)\left(\frac{b}{R}\right)^{2}\right] \quad (5.1)$$

with the geometric function for the mode-I stress intensity factor $F_{\mathrm{I},0}$ for the case of disappearing offset, eqs.(2.1-2.3).

5.2 Offset of the hole exclusively

A second type of non-symmetry is an offset b of the hole with the crack extending in the symmetry line (Fig. 7). This case was studied in detail by He et al.[2] and Lardner et al. [3]. Their results can be expressed for $|b/R| \leq 0.3$ by

$$F_{\mathrm{I}} \cong F_{\mathrm{I},0}\left[1+\left(3.196-0.0835\frac{a}{R}\right)\left(\frac{b}{R}\right)^2\right] \tag{5.2}$$
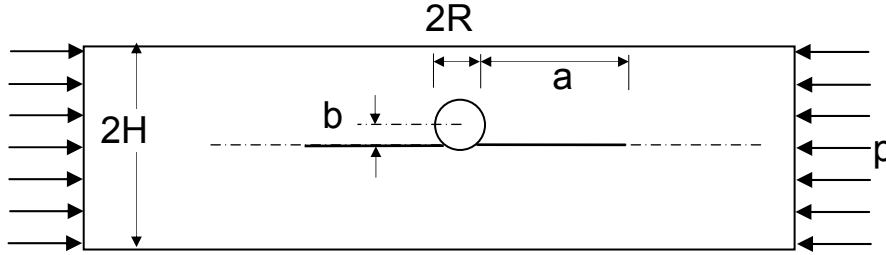

Fig. 7 DCDC specimen with an offset of the hole.

6 Offset of load

If a small non-parallelity between the specimen end and the loading piston of the testing machine by a small angle γ occurs, misalignments in load application result. In addition to the hardly affected normal force, $P_{\mathrm{n}}=P\cos\gamma$, an additional bending moment M_{b} occurs (Fig. 8a). As the consequence, the crack plane may occur rotated by a small angle φ with respect to the symmetry axis. (Fig. 8b). In the contact problem of a hard piston on a hard DCDC-specimen, this additional moment is practically unavoidable since the distance between load P and specimen centre line remains roughly the half specimen width H.

The additionally applied bending moment remains constant during crack extension. Consequently, it will not loose an influence after crack growth as is the case for disturbances caused by the drill hole.

The only efficient way to avoid misalignments in load application seems to be a load introduction via a spherical specimen end part. The authors recommend load introduction via a metal half-sphere into the upper specimen end face as illustrated by Fig. 9. The half-sphere is centred by a short section of a metal tube with slightly larger inner diameter than the specimen cross section diagonal. The tube segment is glued to the specimen with a droplet of epoxy resin.
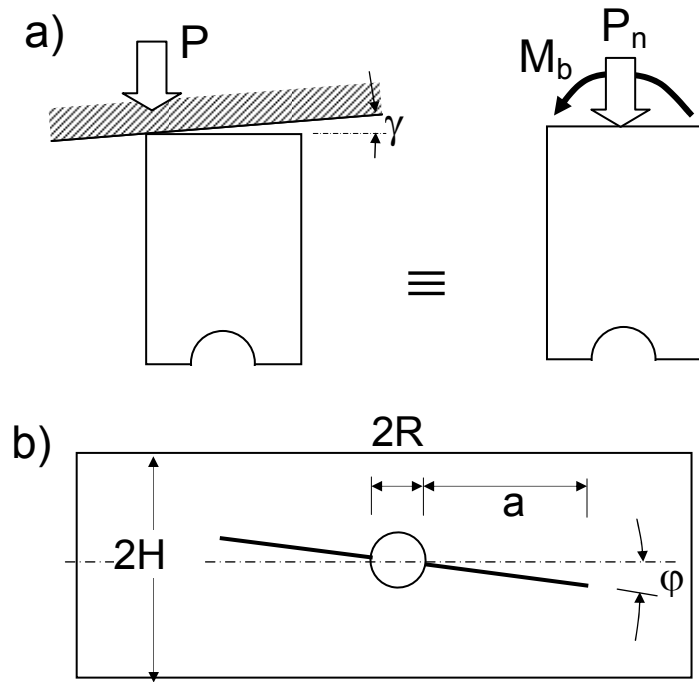
Fig. 8 a) Offset of the load P results in a nearly unchanged central force P_n and a bending moment M_b; b) Consequence of the combined loading is a crack plane tilted by an angle of φ.
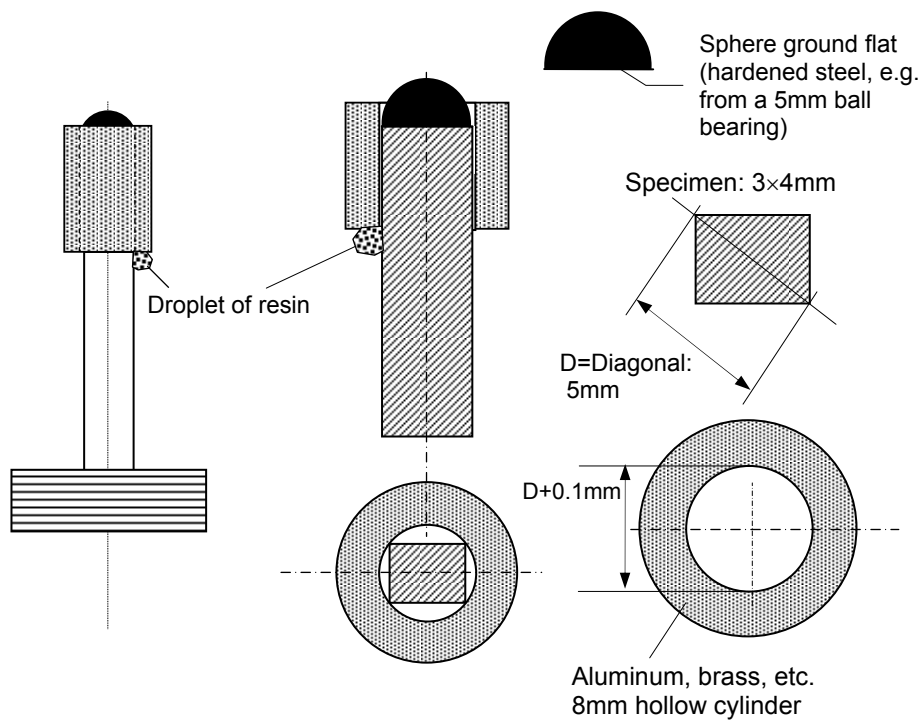
Fig. 9 Load introduced to the DCDC-specimen via a half-sphere; central location of the half sphere guaranteed by a metal tube segment having a diameter slightly larger than the specimen diagonal.

References

1 Janssen, C., Specimen for fracture mechanics studies on glass, in Proceedings Xth International Congress on Glass, (1974), p. 23, Kyoto, Japan.

2 He, M.Y., Turner, M.R., Evans, A.G., Analysis of the double cleavage drilled compression specimen for interface fracture energy measurements over a range of mode mixities, Acta metall. mater. **43**(1995), 3453-3458.

3 Lardner, T.J., Chakravarthy, S., Quinn, J.D., Ritter, J.E., Further analysis of the DCDC specimen with an offset hole, Int. J. Fract. **109**(2001), 227-237.

4 T. Fett, G. Rizzi, D. Munz, T-stress solution for DCDC specimens, Engng. Fract. Mech. **72**(2005), 145-149.

5 Fett, T., Stress intensity factors, T-stresses, Weight functions, IKM 50, Universitätsverlag Karlsruhe, 2008.

6 H. Cai, K.T. Faber, E. R. Fuller, Crack bridging by inclined fibers/whiskers in ceramic composites, J. Am. Ceram. Soc. **75**(1992), 3111-17.

7 T.A. Michalske, E.R. Fuller, Closure and repropagation of healed cracks in silicate glass, *J. Am. Ceram. Soc.* **79**[1] 51-57 (1996)

8 Michalske, T.A., Smith, W.L., Bunker, B.C., Fatigue mechanisms in high-strength silica-glass fibers, J. Am. Ceram. Soc., **74**(1991), 1993-96.

9 G. Pallares, l. Ponson, A. Grimaldi, M. Gorge, G. Prevot, M. Cicciotti, Crack opening profile in DCDC specimen, Int. J. Fract. **156**(2009), 11-20.

10 C. G. Sammis and M. F. Ashby, The failure of brittle porous solids under compressive stress states. Acta Metall. **34**, 51l-526 (1986).

11 Fett, T., Rizzi, G., Guin, J.P., López-Cepero, J.M., Wiederhorn, S.M., A fracture mechanics analysis of the double drilled compression test specimen, Engng. Fract. Mech. **76**(2009), 921-934.